Characterization of a radially emitting spray jet in a cylindrical inertial electrostatic confinement plasma source based on particle in cell simulation

Dominik Tiedemann [a,b,*], Patrick Hofmann [a], Georg Herdrich [d], Andreas Pflug [c], Jens Emmerlich [a], Matthias Müller [a], Sven Ulrich [b]

[a] Robert Bosch Manufacturing Solutions GmbH, Wernerstraße 51, 70469, Stuttgart, Germany
[b] Karlsruhe Institute of Technology, Institute for Applied Materials, Hermann-von-Helmholtz-Platz 1, 76344, Eggenstein-Leopoldshafen, Germany
[c] Fraunhofer Institute for Surface Engineering and Thin Films IST, Riedenkamp 2, 38108, Braunschweig, Germany
[d] Institute of Space Systems, University Stuttgart, Pfaffenwaldring 29, 70569, Stuttgart, Germany

Keywords:
Inertial electrostatic confinement
Cylindrical IEC
Particle in cell simulation
Highly ionized plasma
IPVD

A B S T R A C T

This paper investigates the outflow mechanism of a cylindrical inertial electrostatic confinement plasma source using Particle in Cell plasma simulations. Various phenomena such as ion-wall interactions, impact ionization, excitation, and secondary electron generation are considered. Together with a fine time and cell resolution to reveal relevant phenomena. The results indicate a high electron and ion density in front of the cathode at the widest grid opening, which suggests the formation of a cascade-like charge carrier emission, commonly referred to as the "spray jet". Initially, a virtual anode is formed within the cathode grid and is shifted toward the grid opening as time elapsed. Ions are accelerated in the plasma sheath around the cathode and collide with the cathode grids or oscillate through the grid opening. Electrons are accelerated and ionize the background gas at the plasma sheath edge. While the electron flow is disordered within the cathode it forms a cascade-like quasi-neutral plasma at the outlet of the plasma source. Through the formation of a virtual anode the discharge becomes self-sustained. With this simulation results the working principle of the inertial electrostatic confinement plasma source can be derived.

1. Introduction

The inertial electrostatic confinement (IEC) plasma sources are intensively researched for fusion purposes [1–6]. In special configurations, an IEC source with emitting plasma jet can be achieved [7]. Since the last decades the IEC source jet mode is researched for various applications like for space propulsion [2,8]. Within this research, a cylindrical IEC source is investigated with radial emitting jet for surface treatment purposes. However, the jet extraction mechanism is still not completely understood. Former research focuses on the theory, that the electrons leave the cathode center through the widest cathode grid and ionize the background gas outside the cathode [9]. Chan et al. measured through plasma diagnostics a quasi-neutral low energetic plasma and stated, that due to the low ion energy the ions might be generated outside the cathode [10]. Particle in Cell (PIC) simulations from Bhattacharjee et al. [11] of a cylindrical IEC with symmetric grid arrangement shows that a virtual anode is formed inside the cathode. This potential well can be accompanied with multiple potential wells with increase of the cathode voltage. Furthermore, by considering the ion energy distribution function in different zones along the ion trajectory, two ion groups can be differentiated. One group oscillating through the entire cathode and the other within the cathode. Furthermore, the oscillating ions might be already reflected at the virtual anode and not oscillate through the entire cathode, which was already mentioned by Hirsch [4]. The energy of the ions outside the cathode are rather low energetic [11]. Within the ESA Advanced Concept Team Ariadna study [12], the effects and phenomena leading to beam extraction in a spherical electrostatic inertial confinement device were investigated. For this purpose, simulations based on the Particle in Cell (PIC) method were performed to describe the kinetic behaviour. A Direct Simulation Monte Carlo (DSMC) method was used to model particle motion and electron-induced ionization, and a Fokker-Planck solver was used to model the velocity relaxation of the charge carriers. The Fokker-Planck method describes the diffusion of particles in a plasma without the explicit interactions between the particles, but on the basis of probability distributions. In contrast, the simulations carried out here includes

* Corresponding author. Robert Bosch Manufacturing Solutions GmbH, Wernerstraße 51, 70469, Stuttgart, Germany.
E-mail address: Dominik.Tiedemann@de.bosch.com (D. Tiedemann).

particle interactions, which could be an important factor to describe involved pendulum and extraction mechanism of the charge carriers. This can be seen for example in a multiscale simulation of hollow cathode discharge [13]. The ESA ACT Ariadna study [12] showed that mainly electrons leave the cathode through the jet and no ions are extracted. However, the internal charge carrier distribution and the general function could not be clearly investigated due to the high computational effort of the full electrodynamic description of the processes and the simplifications chosen. This work shows a PIC simulation of a cylindrical IEC source with radial jet emission in addition to the previous studies. The configuration and setup of the cylindrical IEC source was already introduced in former studies [7]. Furthermore, the flux of the electrons and ions as well as their density contour plot of the entire source are shown in a two-dimensional cross section of the introduced cylindrical IEC source. On this basis, a model for the main ion and electron flow inside and outside the cathode was created, which also takes into account the effect of the formation of the virtual cathode for spray-jet operation.

2. Methods and setup

Within the scope of the present work, a probabilistic electrostatic Particle-in-Cell Monte-Carlo (PICMC) code of the Fraunhofer Institute for Surface Engineering and Thin Films (IST) is used for the simulation of the kinetic behaviour of the charged species [14,15]. The basis sequence steps of the PICMC main loop is explained in Fig. 1 in analogy to Bird [16], Birdsall, Langdon et al. [17], Hofmann [18], Vahedi and Surendra [19]. For the simulation time t_{sim} has to be divided into discrete time steps Δt. This is followed by an initial, uniform distribution of the charge carriers into the cells, namely electrons and ions which are represented by super particles with a statistical weight factor. After the initial distribution of the charge carriers into the respective cells, the charge carriers are weighted according to their cell position. Fig. 2 shows an example of a two-dimensional weighting scheme with a macro-particle.

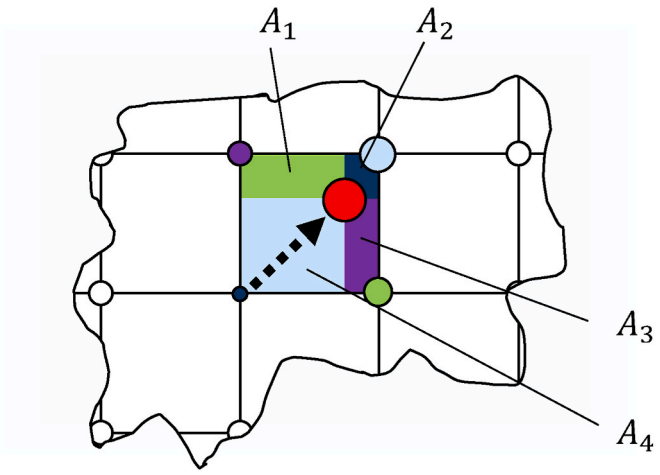

Fig. 2. Exemplary two-dimensional weighting scheme, in which the charge is distributed to the respective nodal points depending on the particle position [18].

In order to assign the charge of the particle to the corresponding net nodes, the net node must be segmented into matching areas A_i. From the segmented areas, the weighting of the macroparticle position to the respective net node is calculated by the following equations:

$$A_1 = h_x \cdot (1 \quad h_y) \tag{2.1}$$

$$A_2 = (1 \quad h_x) \cdot (1 \quad h_y) \tag{2.2}$$

$$A_3 = (1 \quad h_x) \cdot h_y \tag{2.3}$$

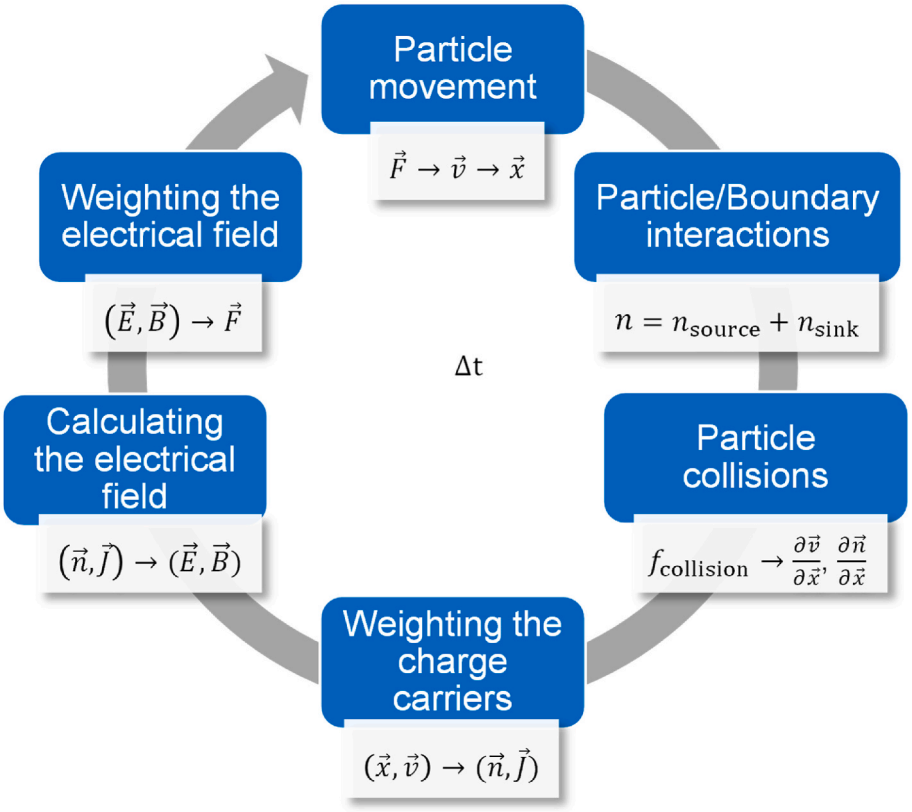

Fig. 1. Sequence diagram of a time step of a particle in cell algorithm. Adapted from [16,18,19].

$$A_4 = h_x \cdot h_y \tag{2.4}$$

Here h_x and h_y are the movement of the macro-particle in x and y direction with respect to the cell origin. Based on the weighting, the potential at the respective net node can be determined in the next step from the sum of all charge carriers within a cell. This allows the assignment of the electric field to the respective computational nodes and the calculation of the movements for the individual macro particles. At the new position, a check of the boundary/particle interactions takes place. This includes, for example, the inflow of new particles via the borders as well as the absorption of particles. In the next step, the impact probability is evaluated for all particles located in a cell. This leads to the change in momentum of the macro-particles. Due to the significantly larger mobility of electrons compared to, for example, ions, a movement of the heavy particles is not necessary in every time step [17,18].

For the PIC simulation, an IEC source setup with eight cathode rods was chosen, which has already been investigated experimentally by Tiedemann et al. [7] and is shown in Fig. 3. The cathode diameter is 30 mm and the exit angle for the jet mode is 80° and is located at the bottom negative z direction. The vacuum chamber acts as an anode and completely encloses the IEC source at a distance of 500 mm.

The center of the coordinate system of the z- and x-axes is located in the geometric center of the IEC source. The IEC source for coating applications presented by Tiedemann et al. [7] is placed between the chamber wall and the substrate. The jet beam of the IEC source is directed towards the substrate for plasma surface treatment. Therefore, the negative z-axis points in the direction of the substrate and the chamber is in the positive z-axis direction.

A cathode voltage of 2 kV and an argon pressure of 3.2 Pa was chosen as initial condition. In the final application of this plasma source, the base pressure of the residual gas will remain in the magnitude of 10^{-4} Pa and is therefore not considered in this simulation. For the corresponding plasma reactions argon atoms, argon ions, excited argon particles and electrons are taken into account. Due to the large chamber volume relative to the size of the source, the argon species are considered to be in a frozen state. This saves computational capacity while still allowing for the consideration of collision interactions. In addition, plasma-wall interactions through a secondary electron emission rate of 0.1 are considered. Electrons will be absorbed at the cathode wall when overcoming the cathode potential. In this configuration, pressure and voltage the cylindrical IEC source works in "spray jet" mode, which was observed experimentally in an industrial coating facility [7]. In the "spray jet" mode, a cascade of charge carriers is emitted from the source. With the cylindrical IEC shape the spray jet emits along the orifice line, that leads to a scalable plasma board with the source length.

2.1. *Influence of cell dimensions on the simulation*

From a 3D model of the IEC source, a 2D slice plane is extracted that intersects the cylindrical IEC source exactly in the middle of the height, along the diameter, and divides the simulation volume into two equal halves. The simulated time span was 5 ms, the grid size was 0.5 mm to resolve the fine movement patterns of the electrons and the time step width was $1 \bullet 10^{-12}$ s to ensure that the mean particle travel distance per time step is below the cell spacing.

The dimensions of a cell in the simulation depend heavily on the charge carrier density and the acceleration voltage. In the present case, a time step of 10^{-12} s and a cell resolution of 0.5 mm were selected to model the entire chamber. Small-scale mechanisms, such as turbulence that could contribute to the exit of a spray jet, can be averaged out by the chosen cell size and the sequential nature of the code. Each displayed contour result corresponds to a temporal and spatial averaging of the quantities, which are then redistributed to the nodes (see Fig. 2). This averaging also smooths out small-scale turbulence, necessitating a very small time step to avoid additional damping effects. With a time step of 10^{-12} s, all relevant phenomena can be temporally resolved, although the gyration motion of electrons becomes less smooth. Furthermore, if the cell resolution is too coarse, the use of a plasma sheath model may also be necessary. At the used voltage range, the plasma sheath is on the order of 0.5 mm, so this resolution is considered sufficient and additional plasma sheath model is required.

3. Results

Fig. 4 displays the electron density (Fig. 4a) and electron energy (Fig. 4b) along the z-axis. A contour plot illustrating the simulated electron density of the cylindrical IEC source is depicted in Fig. 4c. The contour plot shows that the plasma sheaths around each cathode grid

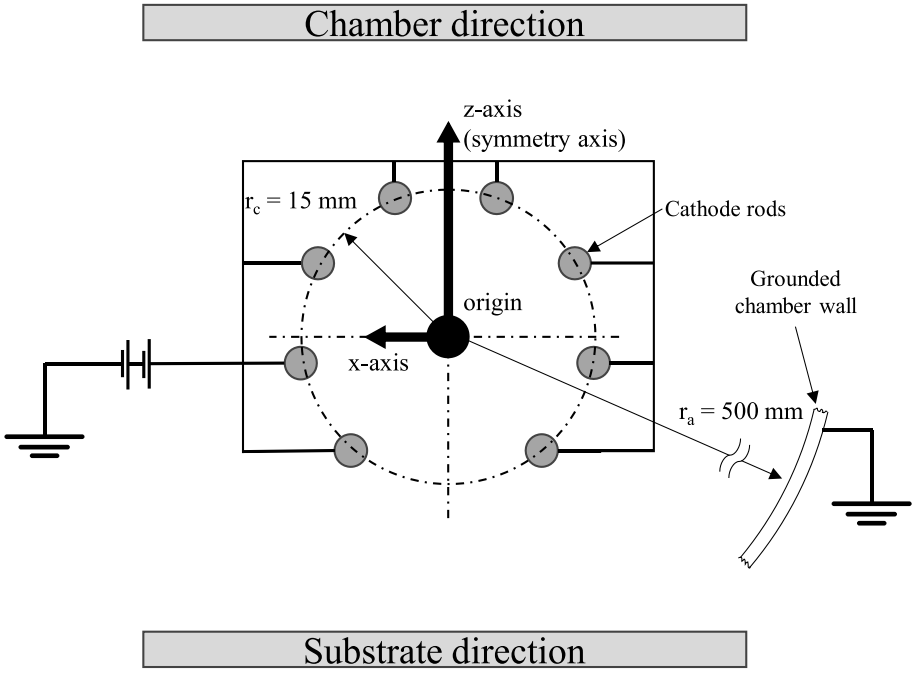

Fig. 3. Grid configuration of the cylindrical IEC source with 8 cathode rods, a diameter of 30 mm and 80° grid opening for the jet mode.

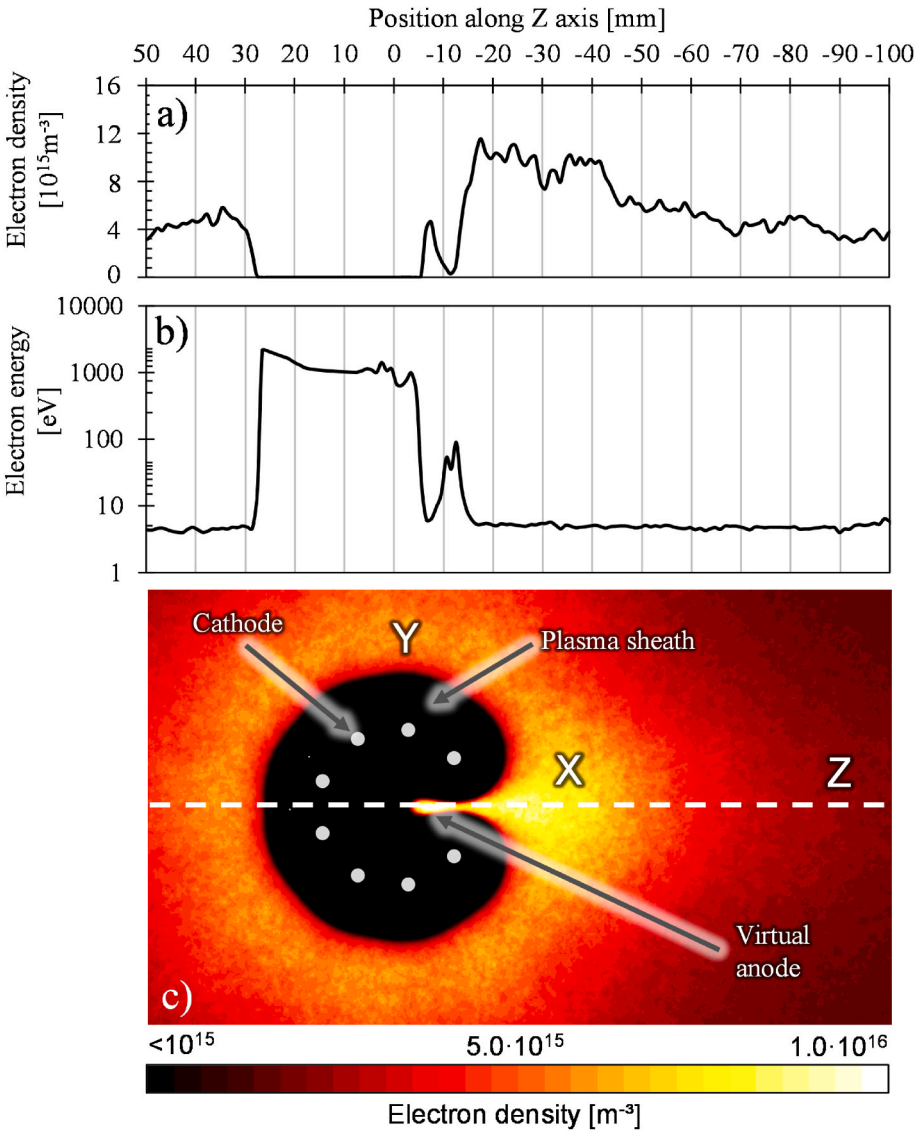

Fig. 4. Cross section of simulated c) electron density in the cylindrical IEC with a) electron energy distribution and b) electron density distribution along the symmetry line of the source.

overlap, resulting in a uniform plasma sheath around the cathode. However, due to high electron density, the plasma sheath overlap is disrupted at the wider grid opening, which is the direction of jet extraction. The electron density within the plasma sheath is lower than that of the bulk plasma. The simulation indicates a dense electron region of up to $1 \bullet 10^{16}$ m ^{3} inside the cathode at z= 6 mm. At the sheath edge around the cathode, the plasma density is half the density of the output region.

The electron density along the z-axis of the symmetry (Fig. 4 above) shows that the density from z=50 mm to z=30 mm gradually increases, while the electron energy is approximately 4–5 eV. From approximately z=27 mm to z=15 mm the electron density decreases to $5 \bullet 10^{15}$ m ^{3}, and the energy decreases along the plasma sheath from around 2000 eV – 1100 eV. Moreover, the electron density remains low inside the cathode until 5 mm, while the electron energy in this region reaches up to 1364 eV. At z= 6 mm, the simulation indicates an electron density peak of up to $4.7 \bullet 10^{15}$ m ^{3}, with an electron energy of around 6 eV. Between this peak and the cathode diameter at z= 15 mm, the density decreases, and the electron energy increases up to 45 eV. After the cathode diameter at around z= 16 mm, the electron density increases again up to $1.4 \bullet 10^{16}$ m ^{3} and decreases continuously to $3 \bullet 10^{15}$ m ^{3} towards z= 100 mm. The electron energy remains around 5 eV in this region.

Fig. 5 presents the results of the simulation of a singly charged positive argon ion. The density of the ion is depicted using a contour plot (see Fig. 5 c)), while the ion energy distribution (see Fig. 5 b)) and ion density distribution (see Fig. 5 a)) along the symmetrical axis are shown in a line plot above. The density at the source orifice is one order of magnitude higher than that around the cathode. Within the cathode plasma sheath, from a position of z=27 mm to z=15 mm, the energy of the singly charged argon ion increases from approximately 1 eV – 550 eV Within the cathode grid, from z=15 mm to z=0 mm, the energy of the singly charged argon ion varies between 35 eV and 130 eV. However, the argon ion density remains constant at approx. $1 \bullet 10^{15}$ m ^{3} between z=27 mm and z=0 mm.

The line plot in Fig. 6 displays the densities of both electrons and singly charged argon ions along the symmetry axis. As shown in Fig. 6 the electron and ion density exhibit a peak of $5.5 \bullet 10^{15}$ m ^{3} and $1.8 \bullet 10^{16}$ m ^{3}, respectively at a distance of z= 6 mm from the source center. As seen from Figs. 4b and 5b the corresponding electron and argon energies are 3 eV and 1 eV, respectively. Furthermore, both densities decrease below $1 \bullet 10^{15}$ m ^{3}, and the energy increases up to 90 eV for

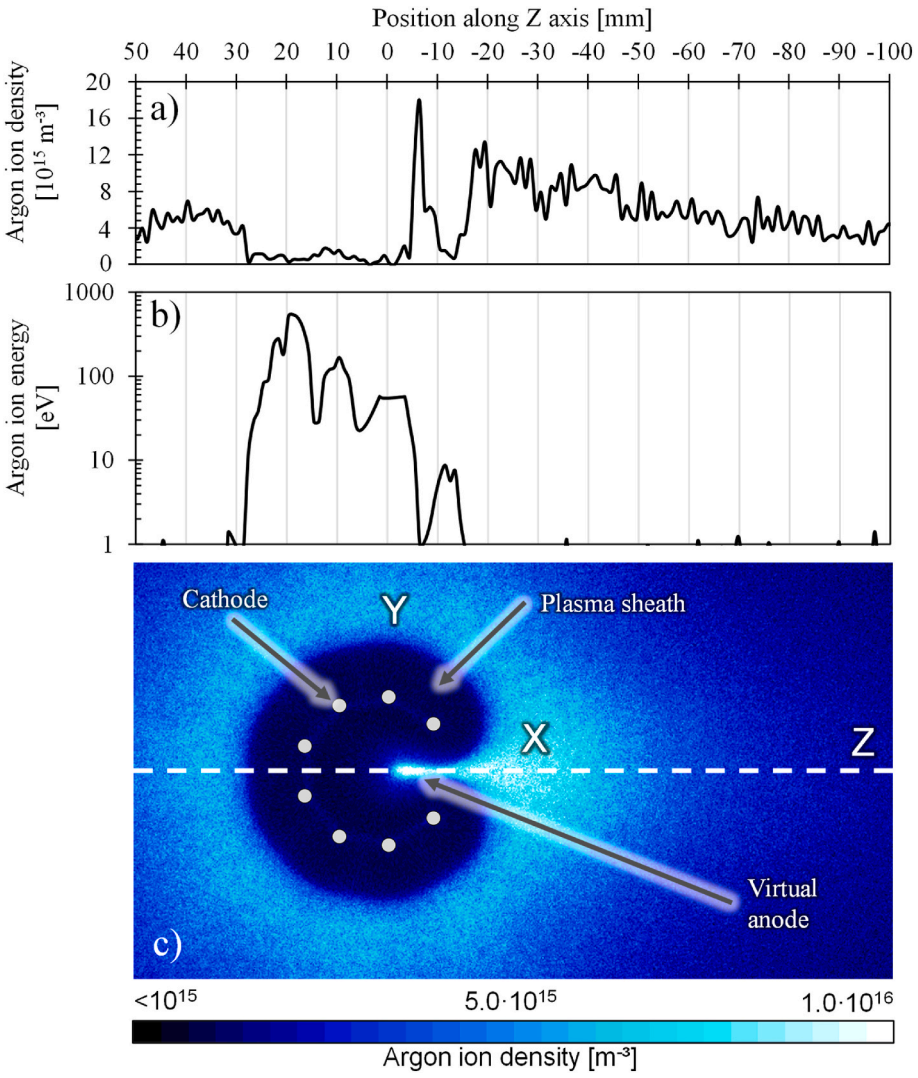

Fig. 5. Cross section of simulated c) argon ion density in the cylindrical IEC with a) argon ion density distribution and b) argon ion energy distribution along the symmetry line of the source.

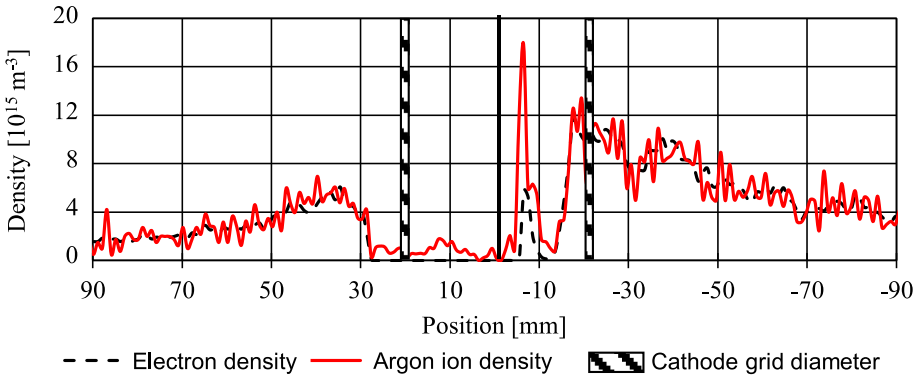

Fig. 6. Comparison electron with argon ion density along the symmetry axis.

electrons and 9 eV for ions in between position z= 8 mm and z= 15 mm. From position z= 15 mm to z= 90 mm, the density for single charged argon ions and electrons first increases to $1.3 \bullet 10^{16}$ m ^{3} and then gradually decreases with increasing distance from the cathode to $3 \bullet 10^{15}$ m ^{3} at z= 90 mm.

By examining the plot in Fig. 6, it is evident that the densities for both species are the same within the region of z=90 mm to z=30 mm and from z= 16 mm to z= 90 mm. However, there is an imbalance in the densities within the plasma sheath and cathode. In this region, the density of singly charged argon ions is higher than that of electrons. At the peak position of z= 6 mm, the density of singly charged argon ions is three times higher than that of electrons. Consequently, the peak will

be considered as a virtual anode, owing to the higher ion fraction.

Fig. 7 depicts the flux of singly charged argon ions and electrons along the symmetry axis of the source (refer to Figs. 4 and 5 for comparison). The plot only represents the flux direction along the symmetry axis. Negative fluxes indicate that the ions or electrons move towards the jet output that is directed towards the substrate. In contrast, positive fluxes indicate that the particles move in the opposite direction, towards the chamber. The cathode diameter is also shown, which is ±15 mm. Within the range of z=30 mm to z=15 mm, the plasma sheath accelerates the ions towards the substrate and the electrons towards the chamber. However, the flux direction changes inside the cathode, with the ions moving towards the chamber and the electrons towards the substrate. Following the virtual anode at position z= 6 mm, the electron flux experiences a sharp increase from z= 6 mm to z= 15 mm and then decreases in the range of z= 15 mm to z= 25 mm. During these regions, the ion flux remains small.

Fig. 8 shows the 2D cross section of the cylindrical IEC source, which includes the simulated electron density contour plot and arrows indicating the electron flux and their direction. For this purpose, the results were averaged over 0.5 ms and combined to this superimposed representation. The contour plot reveals that in the outer plasma sheath, electrons leave in channels directed outwards from the cathode center. Within the cathode, electrons flow without any specific direction. To observe the electron flow in the plasma jet, a different scale of the flux without the background density plot was selected (see Fig. 9). The simulation indicates that a major part of the electron flux originates at the virtual anode location (Fig. 4, position z= 6 mm). From there, the electrons leave the cathode circle via an almost unidirectional jet towards the substrate. Outside of the cathode circle, the flux orientation becomes more disordered. In general, the flux at the jet output is higher than the flux at the sheath edge around the cathode.

Fig. 10 displays the 2D cross section of the cylindrical plasma source, illustrating the single charged argon ion flux. To achieve this, the interim results were averaged over a 0.5 ms duration and then integrated into this composite representation. The background contour plot shows the ion density, and arrows indicate the ion flux and their direction. The simulation reveals that in the outer plasma sheath, the ion flux is directed towards the source center and increases as it approaches the cathode grids. Within the cathode, the ion flux is directed towards the cathode grids away from the virtual anode (see Fig. 4 at position z= 6 mm). The ion flux in the direction of the jet exit is low at the virtual anode, and in the region of high ion density in front of the cathode, the flux is comparatively low, similar to the inner cathode region. Unlike the electrons flowing in channels between the two rods at the output, the ions are not emitted from the geometrical center of the entire cathode configuration but are accelerated toward the cathode rods.

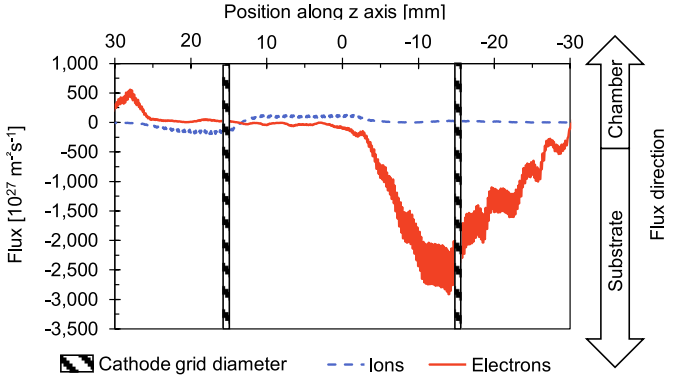

Fig. 7. Comparison of the argon ion and electron flux along the symmetry axis of the source. Additionally, the Cathode diameter is illustrated and the flux direction.

Fig. 11 shows the potential distribution of the cross section (c), with line plots above depicting two horizontal sections of the potential (a). One section passes through the geometrical center of the entire cathode configuration, while the other passes through the virtual anode located inside the cathode (see Fig. 4, position z= 6 mm). The potential distribution along the symmetry axis is illustrated on the right side of the figure (b). The horizontal axis section shows that the electrical potential decreases in the plasma sheath from 30 mm to 15 mm, and from 15 mm to 30 mm. Inside the cathode, the potential increases as it approaches the cathode center. The potential peak in the cathode center reaches 600 V, while it is 26 V in the virtual anode. However, the potential distribution is not symmetric along the vertical symmetry axis. In the direction of the jet output, the potential drops to 26 V at the virtual anode after passing the cathode diameter. The potential then decreases continuously to approximately 3 V.

The motion trajectory of randomly selected ions in a 0.5 ms time frame is shown in Fig. 12. Each point on the plotted path represents a position of the corresponding ion at a given time. Several time steps elapse between the individual points, with the change in size indicating the change in position and the rate of change in diameter being an indicator of acceleration. The simulation reveals that ions are accelerated from the outer plasma sheath towards the cathode center. Ions with trajectories between the grids are more likely to pass the cathode and be directed towards the center, while those with trajectories close to the cathode grid are more likely to be collected by the grids. The number of ions colliding with the cathode grid is higher at the two extraction grids for the spray jet, but no extraction of ions from the cathode center is observed.

Fig. 13 shows an enlarged section of the electrical potential, electron and ion density within the virtual anode and cathode along the z-axis. The corresponding electrical potential reveals the movement direction of ions and electrons in three sections due to an imbalance of charge carriers. In section I, electrons move towards the cathode outlet, while ions move towards the cathode center. Due to the high ion density in position z= 6 mm and a further increase of the electron density as well as a decrease of the ion density towards position z= 11 mm, a potential well is formed which confines the low-energy electrons. In section II, electrons generated in this region are accelerated towards the virtual anode, while ions are accelerated towards the source outlet. In section III, quasi-neutrality in charge carrier densities causes the electric potential to drop further to the plasma potential of around 4 V. Between sections II and III, another potential well is formed, trapping low-energy ions. The formation of the electric potential in section IIcould indicate an ambipolar diffusion mechanism that could cause ionization, thus producing ions and electrons in this region. Section IIIsuggests that ions are more likely to be accelerated towards the cathode center and not extracted by the source through the jet.

4. Discussion

The electric field between the cathode rods of the IEC source and the chamber wall initiates a plasma discharge, which in turn creates an electric field within the cathode grid. Due to the imbalance in the ion-electron ratio, a virtual anode is formed. The electrical potential distribution is similar to the simulated and measured potential distribution reported by Bhattacharjee et al. [20], who investigated a highly symmetrical cylindrical inertial electrostatic confinement plasma source for fusion application. The validation of their simulation was conducted using Langmuir probe measurements. Qualitatively, the spatial distribution of the electrical potential shown in this work aligns with the findings reported by Bhattacharjee et al. In this work, a similar potential distribution can be observed, but shifted towards the jet outlet.

The simulated electrical potential in Fig. 11 shows that the ion density at the virtual anode increases the electrical potential to 26 V. The higher ion content is caused by ions entering from the plasma discharge outside the cathode through the cathode grid openings, as the

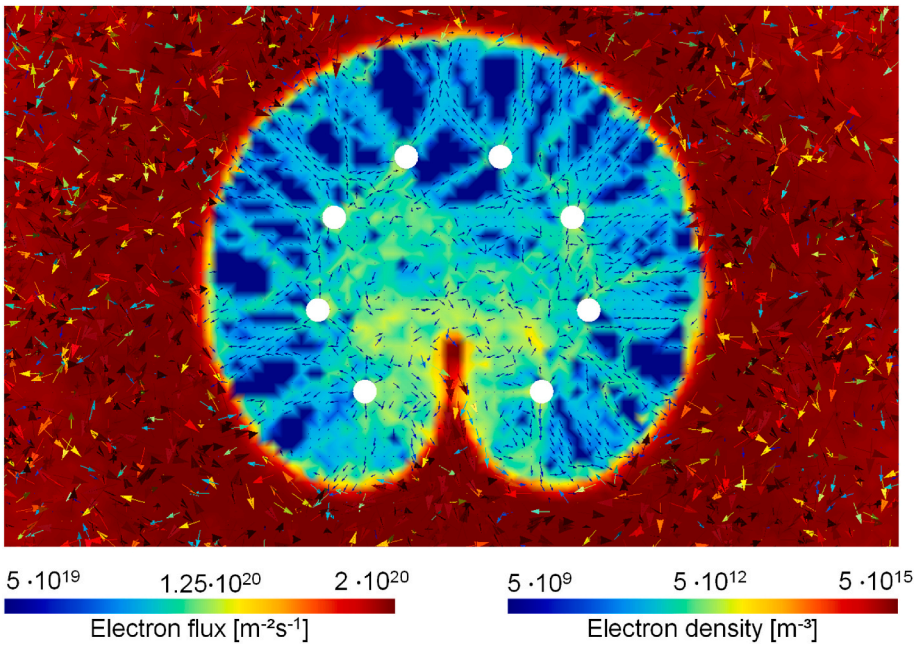

Fig. 8. contour plot of the species path and the corresponding velocity vector within the cylindrical IEC plasma source including the plasma sheath.

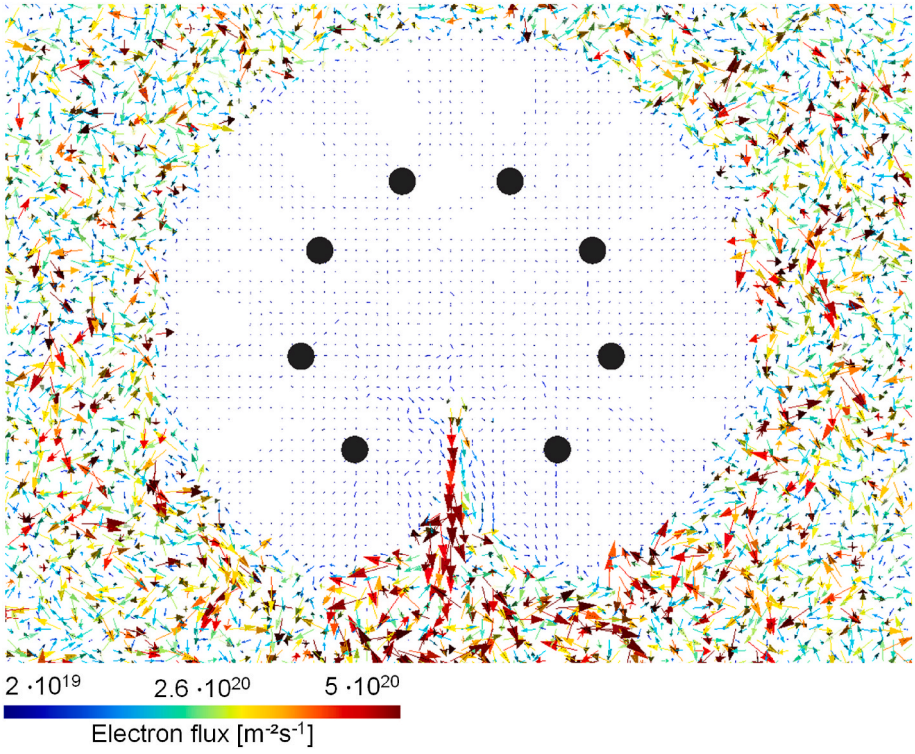

Fig. 9. Simulated electron flux at the grid opening of the cylindrical IEC plasma source.

trajectories are showing in Fig. 12. The potential barrier created by the cathode acts as a filter, allowing only ions to enter the cathode center from outside. Conversely, electrons can only exit the cathode through an electron jet located at the widest grid opening, resulting in a decrease in electron density within the cathode. The virtual anode and resulting electrical field cause the acceleration and deceleration of charge carriers. The negative voltage applied to the cathode creates a high potential barrier that prevents electrons outside the cathode grid from entering or leaving through the grid openings, except in the spray jet outlet area. This can also be seen in the electron flux in Fig. 8 which shows that the electron flux originates from the cathode grids. The flux direction points either inwards or outwards the cathode grids. Therefore, only electrons generated inside the cathode grid, such as from secondary electron emission due to ion bombardment or impact ionization, can contribute to the discharge inside the cathode. Due to the electrical field inside the cathode caused by the virtual anode the electrons within the cathode grid are moving in a pendulum motion. This behaviour can also be observed in hollow cathode discharges [21],

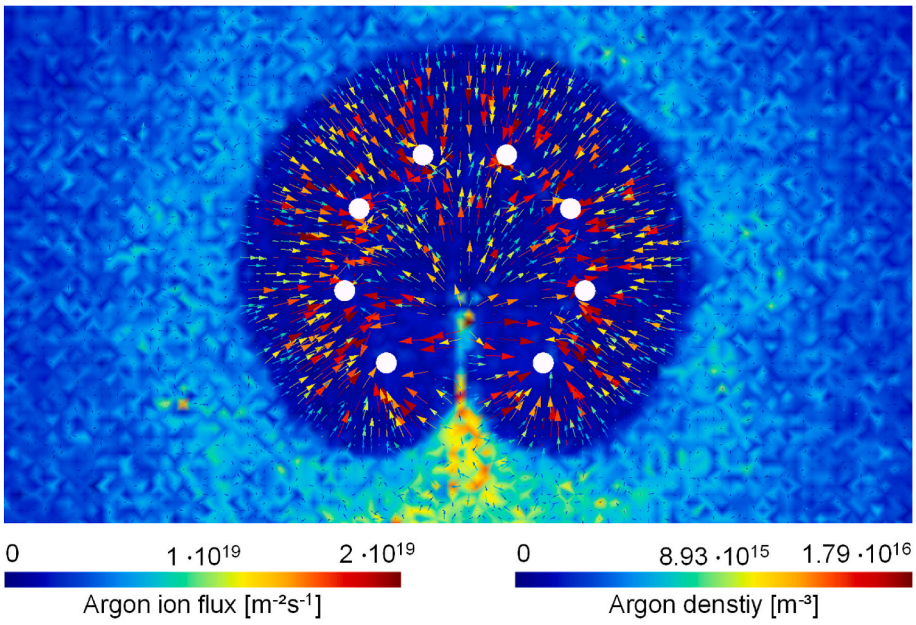

Fig. 10. Simulated argon ion flux and density within the cathode of the cylindrical IEC plasma source including the plasma sheath.

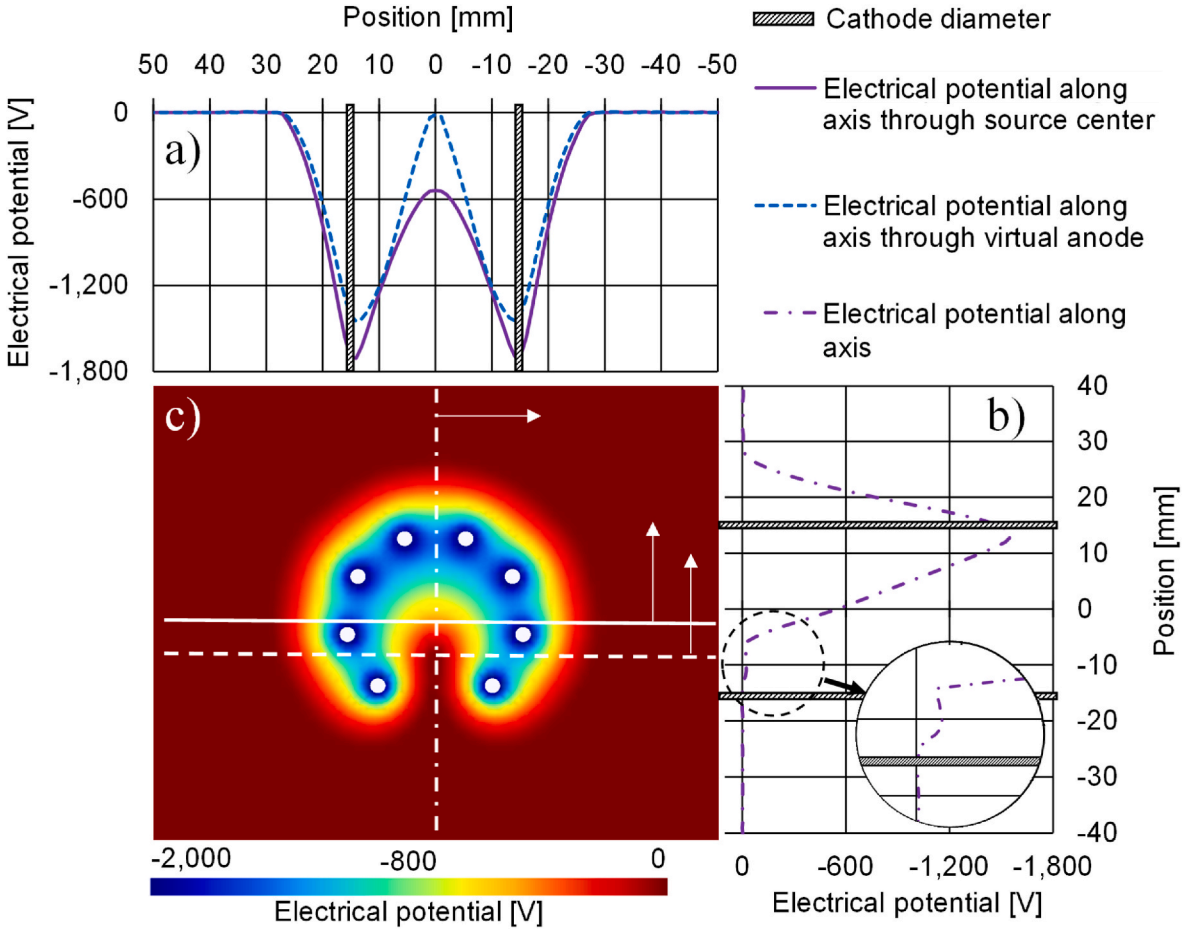

Fig. 11. Simulated electric potential distribution of the cylindrical IEC plasma source cross section c) with intersection lines along the symmetry axis b) and perpendicular through the source center and the dense plasma region close to the grid opening a).

where such faster electrons are forced to a longer trajectory and therefore leads to a stronger impact ionization of the background gas species. The existence of such pendulum mechanism theory has also been mentioned in literature [10]. The electrical barrier for electrons is lower at wider grid openings, creating a weak spot allowing electrons leave the electrostatic confinement. This escape occurs in a collimated flux, taking

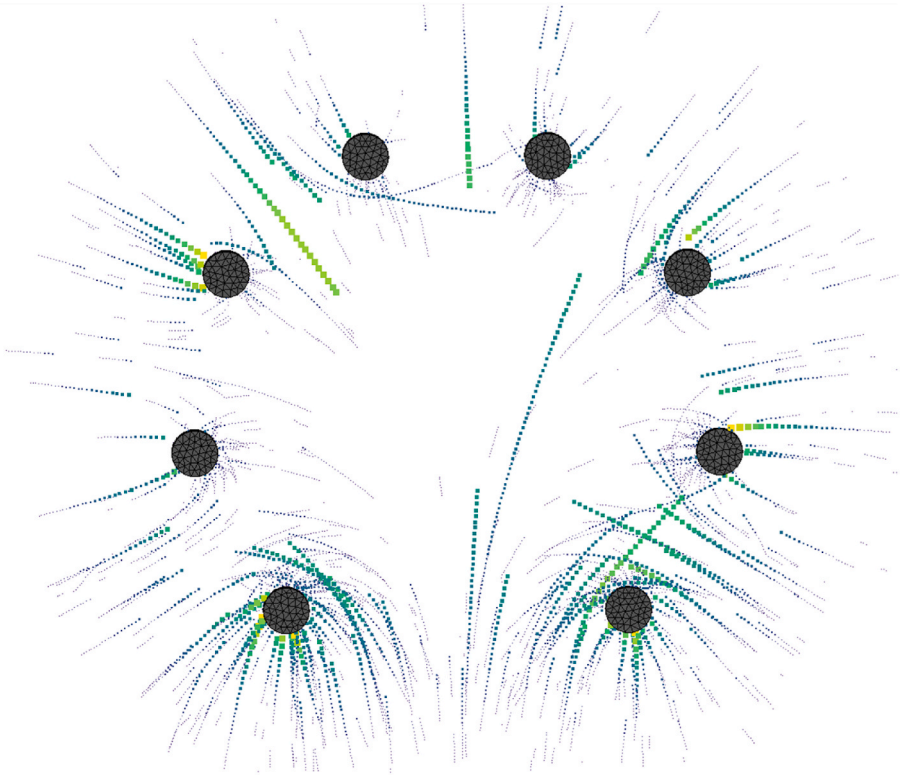

Fig. 12. Movement of the ions at the cylindrical IEC plasma source operated in spray jet mode.

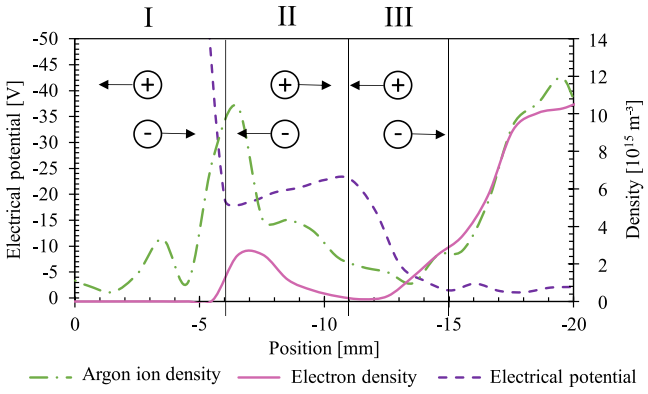

Fig. 13. Charge carrier movement within the cathode grid due to the virtual anode and cathode.

the shape of an electron jet, as shown in Fig. 9. This supports the theory of Chan et al. that only electrons can leave the cathode center and the ions of the spray jet are generated outside the cathode [22–24]. The virtual anode can only be sustained as long as electrons are continuously provided, and a higher fraction of electrons leave the cathode through the jet. The electrical potential decreases along the z-axis, i.e. the symmetry line of the source (see Fig. 11). It remains at a low potential from the virtual anode towards the jet output due to the high ion fraction. Consequently, with a higher ion fraction at the virtual anode and in the mentioned channel the electrical barrier for electrons is reduced enabling electron extraction through the jet with lower energies. The strong potential gradient within the cathode forces incoming oscillating ions to return towards the cathode grids before they reach the cathode center. This simulated behaviour supports the theory proposed by Miley and Murali [1], which claims that ions from outside the grid contribute to the formation of the virtual anode. It is important to note that PIC simulations only show small timeframes of the ignition and maintenance of the plasma and does not reflect the long-term variation of plasma properties over time.

4.1. Critical examination of the exit mechanism considering numerical constraints

In the simulation, the background gas was assumed to be stationary since the velocity of the gas is significant slower compared to the charge carriers. This assumption is considered reasonable to save computation time with only a minor loss in accuracy. However, phenomena such as impact ionization and secondary electron generation were considered, allowing ionization of the charge carriers within the IEC source and leading to an increase in electrons and ions within the source.

4.1.1. Simulation procedure and collision detection in the particle-in-cell (PIC) method

As previously detailed, the simulation procedure involves initially distributing charge carriers randomly within the simulation volume. These carriers then move under the influence of the applied potential and collisions. In the absence of initial charge carriers and background gas (argon), simple exit of charge carriers would be conceivable. However, accelerated electrons generate a collision cascade in front of the source, similar to a Townsend discharge. The ions, being less volatile, contribute to the desired pendulum movement within the source. For ions to escape the potential well, an additional counter-pole would be required to extract the ions. This has already been experimentally confirmed in the deployment of a coating system and through simulation [25–27], though it falls outside the scope of this work.

In the Particle-in-Cell (PIC) method, particles are allowed free movement. The Cartesian grid is only used to detect collisions. In the event of a successful collision, new particles are generated at the origin coordinates of the collision or deflected from this position. For successful collision detection, particles must reside in a cell for at least one time step to prevent cell hopping or numerical heating.

4.1.2. Challenges in achieving stationary states with particle-in-cell codes

Due to the use of a Particle-in-Cell code, a stationary state is not reached. Instead, time spans are typically chosen based on empirical values [13–15,28] and checked to see if significant changes in quantities occur over the last multiple time steps. However, the design of the IEC source quickly leads to a relatively high charge carrier density, which is difficult to model with the existing PIC code. With increasing charge carrier density, cell size and time step increments must be adaptively adjusted to prevent cell hopping. This way, charge carrier flows could also be accurately modeled over a long-term simulation up to a stationary state. The newly formed potentials could drive the spray jet exit. However, this is currently not possible due to the immense computational effort. Relief could be provided by implementing so-called hanging nodes to resolve areas near the source more finely.

4.1.3. Challenges and alternative approaches to modeling real IEC sources

Real IEC sources exhibit significantly higher charge carrier densities, which cannot currently be modeled with a PIC approach due to the high computational effort (squared particle number effect). At very high charge carrier densities, saturation effects of the electric potential can occur, or new potential wells can form that could favor the exit mechanism.

An alternative approach could be the use of a fluid model. Such simulations, however, require numerous additional assumptions, such as turbulence models, drift velocities, and reaction rates. These assumptions are not required in a PIC simulation, as they are inherently in the nature of the PIC scheme. Nevertheless, the fluid approach could better address the challenges of high charge carrier densities and potentially more accurately model the mechanisms behind the exit, provided suitable turbulence models and assumptions are found.

5. Conclusion

The PIC simulation was used to understand extraction of the jet mode in a cylindrical IEC source. In the chosen configuration a high electron and ion density was observed in front of the cathode at the widest grid opening, which is assumed to be the formation of a spray jet. A virtual anode is formed inside the cathode grid. In comparison to the symmetric grid configuration with no jet mode, this virtual anode is shifted towards the grid opening. Ions are accelerated in the plasma sheath around the cathode and collide either with the cathode grids or oscillate through the grid opening. Inside the cathode, the ions are accelerated away from the virtual anode in direction of the cathode grids. Electrons are accelerated in the plasma sheath around the cathode towards the channels leading away from the cathode center and ionize the background gas at the sheath edge. Within the cathode, the electron flow is disordered. Except for the virtual anode the densities of ions and electrons, respectively, are low in contrast to their high energies. Within the virtual anode the charge carrier densities increase but the mean electron energy is low. The electrons could be derived from impact ionization which results in low energetic electrons. The potential well caused by the ion density results in a self-sustained discharge within the cathode This discharge is very similar to the hollow cathode discharge. The plasma sheaths from each grid overlap except for the two sheaths at the widest grid opening. The space charge of the virtual anode decreases the electrical potential in the channel between these grids enabling the electrons to escape in a collimated channel. Furthermore, the generated ions at the virtual anode and in the electron jet are accelerated through the plasma sheath to the cathode grids. The high ion density in front of the cathode opening might arise from electron impact ionization of the background gas outside the cathode and do not originate from the cathode center. Further research is needed in order to understand the nature of the jet mode. The working principle of the IEC source in jet mode can be derived using this PIC simulation, which shows that electron impact ionization within the source center results in a discharge that triggers the spray jet mode.

CRediT authorship contribution statement

Dominik Tiedemann: Writing – review & editing, Writing – original draft, Validation, Project administration, Investigation, Formal analysis, Data curation, Conceptualization. **Patrick Hofmann:** Writing – review & editing, Visualization, Validation, Software. **Georg Herdrich:** Writing – review & editing, Validation, Conceptualization. **Andreas Pflug:** Writing – review & editing, Visualization, Software. **Jens Emmerlich:** Writing – review & editing, Conceptualization. **Matthias Müller:** Writing – review & editing, Resources. **Sven Ulrich:** Writing – review & editing, Supervision, Conceptualization.

Declaration of competing interest

The authors declare that they have no known competing financial interests or personal relationships that could have appeared to influence the work reported in this paper.

Data availability

No data was used for the research described in the article.

References

[1] G.H. Miley, S.K. Murali, Inertial Electrostatic Confinement (IEC) Fusion, Springer New York, New York, NY, 2014.

[2] G. Herdrich, U. Bauder, A. Boxberger, R.A. Gabrielli, M. Lau, D. Petkow, M. Pfeiffer, C. Syring, S. Fasoulas, Advanced plasma (propulsion) concepts at IRS, Vacuum 88 (2013) 36–41, https://doi.org/10.1016/j.vacuum.2012.02.032.

[3] K. Yamauchi, Y. Takeuchi, Y. Ogino, M. Watanabe, A. Okino, Y. Sunaga, E. Hotta, Neutron production rate and plasma characteristics of spherically convergent beam fusion, Electr. Eng. Jpn. 135 (2001) 1–8, https://doi.org/10.1002/eej.1.

[4] R.L. Hirsch, Inertial-electrostatic confinement of ionized fusion gases, J. Appl. Phys. 38 (1967) 4522–4534, https://doi.org/10.1063/1.1709162.

[5] J. Nadler, Inertial-Electrostatic confinement (IEC) Fusion for space propulsion. https://ntrs.nasa.gov/citations/19990103080, 1999. (Accessed 6 September 2023).

[6] M. Ohnishi, Y. Yamamoto, M. Hasegawa, K. Yoshikawa, G.H. Miley, Study on an inertial electrostatic confinement fusion as a portable neutron source, Fusion Eng. Des. 42 (1998) 207–211, https://doi.org/10.1016/S0920-3796(97)00199-3.

[7] D. Tiedemann, P. Hofmann, J. Emmerlich, Y.-A. Chan, S. Ulrich, G. Herdrich, M. Müller, Cylindrical inertial electrostatic confinement plasma source for surface treatment, Vacuum 193 (2021) 110502, https://doi.org/10.1016/j.vacuum.2021.110502.

[8] C. Syring, G. Herdrich, Experimental Discharge Characterization and Scaling of IEC Plasma Devices, the 33rd International Electric Propulsion Conference, The George Washington University, USA, 2013.

[9] J. Nadler, E. Yoder, C. Hunsicker, G. Miley, Experimental Investigation of Unique Plasma Jets for Use as Ion Thrusters, American Institute of Aeronautics and Astronautics, 1998, https://doi.org/10.2514/6.1998-2570.

[10] Y.-A. Chan, G. Herdrich, Influence of cathode dimension on discharge characteristics of inertial electrostatic confinement thruster. The 36th International Electric Propulsion Conference, University, of Vienna, Austria, 2019.

[11] D. Bhattacharjee, N. Buzarbaruah, S.R. Mohanty, S. Adhikari, Kinetic characteristics of ions in an inertial electrostatic confinement device, Phys. Rev. E 102 (2020), https://doi.org/10.1103/PhysRevE.102.063205.

[12] G. Herdrich, D. Petkow, C. Syring, M. Pfeiffer (Eds.), Kinetic Modelling of the Jet Extraction Mechanism in Spherical IEC Devices, 2013.

[13] P. Hofmann, R. Gryga, M. Müller, M. Stüber, S. Ulrich, Multiscale simulation of hollow cathode assisted internal plasma treatment process, Surf. Coating. Technol. (2022) 128422, https://doi.org/10.1016/j.surfcoat.2022.128422.

[14] T. Melzig, M. Siemers, A. Pflug, R. Rank, 3D PIC-MC simulation of anode effects in dual magnetron discharges, Surf. Coating. Technol. 241 (2014) 30–32, https://doi.org/10.1016/j.surfcoat.2013.10.024.

[15] M. Turowski, M. Jupé, H. Ehlers, T. Melzig, A. Pflug, D. Ristau, Simulation in Thin Film Technology, 2015 962707, https://doi.org/10.1117/12.2191693.

[16] G.A. Bird, Monte Carlo simulation of gas flows, Annu. Rev. Fluid Mech. 10 (1978) 11–31, https://doi.org/10.1146/annurev.fl.10.010178.000303.

[17] C.K. Birdsall, A. Langdon, Plasma Physics via Computer Simulation, CRC Press, Taylor & Francis, New York, 2018.

[18] P. Hofmann, Simulative Optimierung von plasmagestützten Vakuumbeschichtungsprozessen, Karlsruher Institut für Technologie (KIT), 2023.

[19] V. Vahedi, M. Surendra, A Monte Carlo collision model for the particle-in-cell method: applications to argon and oxygen discharges, Comput. Phys. Commun. 87 (1995) 179–198, https://doi.org/10.1016/0010-4655(94)00171-W.

[20] D. Bhattacharjee, S. Adhikari, N. Buzarbaruah, S.R. Mohanty, PIC simulation of particle behavior in an Inertial Electrostatic Confinement Fusion device using XOOPIC code, Plasma Phys. (2020). https://api.semanticscholar.org/CorpusID:211126891.

[21] S. Muhl, A. Pérez, The use of hollow cathodes in deposition processes: a critical review, Thin Solid Films 579 (2015) 174–198, https://doi.org/10.1016/j.tsf.2015.02.066.
[22] Y.-A. Chan, G. Herdrich, Inertial electrostatic confinement: innovation for electric propulsion and plasma systems. The 35th International Electric Propulsion Conference, Georgia Institute of Technology, USA, 2017.
[23] Y.-A. Chan, G. Herdrich, Back-vacuum retarding potential analyzer for investigation of plasma properties from inertial electrostatic confinement thruster. The 36th International Electric Propulsion Conference, University, of Vienna, Austria, 2019.
[24] C. Syring, G. Herdrich, M. Zürn, Thrust Model and Analytical Assessment of Losses in IEC Devices, 5th Russian German Conference on Electric Propulsion, 2014.
[25] D. Tiedemann, P. Hofmann, R. Gryga, J. Emmerlich, M. Müller, G. Herdrich, S. Ulrich, Influence of cathode grid geometry on the operation behaviour of cylindrical inertial electrostatic confinement plasma sources in jet mode, V2023 - vacuum Plasma Surface Coating. International Conference & Exhibition, Internationales Congress Center Dresden, Research Poster Dresden, Internationales Congress Center Dresden, Research Poster, 2023.
[26] D. Tiedemann, J. Emmerlich, P. Hofmann, M. Müller, G. Herdrich, S. Ulrich (Eds.), Optimized Cylindrical Electrostatic Confinement Plasma Source for Thin Film Applications, Plathinium 2023 Plasma Thin Film International Union Meeting, Paris, 2023.
[27] D. Tiedemann. Entwicklung einer Niederdruck Plasmaquelle nach dem Prinzip des elektrostatischen Trägheitseinschlusses zur Oberflächenbehandlung in industriellen Anwendungen, Karlsruher Institut für Technologie (KIT), 2023, https://doi.org/10.5445/IR/1000164434.
[28] M. Siemers, A. Pflug, B. Szyszka, Three Dimensional Plasma Simulations with a Parallelized Particle-In-Cell Monte Carlo Approach, 2006.